Hindawi Publishing Corporation
Journal of Nanomaterials
Volume 2013, Article ID 762381, 9 pages
http://dx.doi.org/10.1155/2013/762381

Research Article

Preparation and *In Vitro* and *In Vivo* Performance of Magnesium Ion Substituted Biphasic Calcium Phosphate Spherical Microscaffolds as Human Adipose Tissue-Derived Mesenchymal Stem Cell Microcarriers

Dong-Hyun Kim,[1] Tae-Wan Kim,[1] Ju Dong Lee,[2] Keun-Koo Shin,[3] Jin Sup Jung,[3] Kyu-Hong Hwang,[4] Jong Kook Lee,[5] Hong-Chae Park,[1] and Seog-Young Yoon[1]

[1] *School of Materials Science and Engineering, Pusan National University, Busan 609-735, Republic of Korea*
[2] *Korea Institutes of Industrial Technology, Busan 618-230, Republic of Korea*
[3] *Department of Physiology, School of Medicine, Pusan National University, Yangsan 626-770, Republic of Korea*
[4] *School of Nano and Advanced Materials, Gyeongsang National University, Jinju 660-701, Republic of Korea*
[5] *Department of Advanced Materials Engineering, Chosun University, Gwangju 501-759, Republic of Korea*

Correspondence should be addressed to Seog-Young Yoon; syy3@pusan.ac.kr

Received 17 April 2013; Accepted 16 May 2013

Academic Editor: Eng San Thian

Magnesium ion substituted biphasic calcium phosphate (Mg-BCP) bioceramic microscaffolds with spherical and porous morphology were successfully prepared using *in situ* coprecipitation and rotary spray drying atomization process for application of tissue engineering combined with human adipose tissue-derived mesenchymal stem cells (hAT-MSCs). After 4 weeks of immersion in Hanks' balanced salt solution (HBSS), Mg-BCP micro-scaffolds showed the enhanced biodegradation and bioactivity due to the substituted Mg^{2+} ion present in the BCP structure. In this study, it was observed that hAT-MSCs have clearly attached on the surface of Mg-BCP micro-scaffolds. In addition, Mg-BCP micro-scaffolds exhibited the improved biocompatibility and osteoconductivity via *in vitro* and *in vivo* biological tests with hAT-MSCs. Therefore, these bioceramic micro-scaffolds had potential to be used as hAT-MSCs microcarriers for biomedical applications.

1. Introduction

Microsized calcium phosphate (CP) spherical bioceramic granules have gained great interest for use as bone grafting cement materials in non-load-bearing situation which means a better filling of an irregular defect and high packing into damaged bone tissues. The main reason is that the bioresorption rate of porous granules could be predicted to be faster than dense blocks made of the same material [1–3]. In addition, uniformly packed spheres with homogenous pore distribution have been reported to increase the rate of bone ingrowth [4]. Tamimi et al. reported that the application of monetite bioceramic granules showed faster resorption and increased bone neoformation when compared with commercial apatite granules from animal source [5]. Paul et al. reported hydroxyapatite ceramic microspheres for use as delivery of insulin [6]. Labbaf et al. reported the interaction between spherical bioactive glass particles and human mesenchymal stem cells [7]. For that reason, spherical CP microgranules can be used either as bone grafting materials, or as carriers for drugs or cells [8–10]. Recently, one of the CP materials in bone grafting bioceramics, biphasic calcium phosphates (BCPs, HAp/β-TCP), has focused on studies for multiphase control and effects of ionic substitutions in order to optimize bioresorbability and bioactivity [11–14]. For example, Mg^{2+} ion-substituted CPs have been reported to enhance bioresorbability and bioactivity during the early stages of osteogenesis where they stimulate osteoblast

proliferation [15, 16]. According to our previous study, it was also shown that the appropriate substitutions of Mg^{2+} ions in BCP powder could accelerate the formation of biological new apatite than pure BCP [17].

Stem cells in bone tissue engineering are also one of the most promising alternatives for existing treatment modalities for bone defects because they could be osteogenic differentiated under *in vitro* and *in vivo* condition. However, they are not subject to supply limitations due to their self-renewal capacity [18]. In addition, the application of embryonic stem cells is strictly limited due to ethical and political issues. In order to solve such complex problems, there have been many recent reports on success of isolating stem cells and osteogenic differentiated from human, rat, rabbit, and mouse adipose tissue sources [19–22].

Most models of bone-tissue scaffold engineering are based on seeding mesenchymal stem cells (MSCs) onto biodegradable and biocompatible three-dimensional (3D) bulk scaffolds like biopolymers, ceramics, and composites. However, 3D scaffolds are very difficult to apply to combining and seeding MSCs inside pore spacing without control of large open pore size (100~500 μm) in bone-tissue engineering. Therefore, usability viewpoint of MSCs could bring out the scaffold application of new concept [23–25]. Here, we describe for the first time the successful formation of mineralized bone tissue by the combination of Mg^{2+} ion-substituted biphasic calcium phosphate (Mg-BCP) spherical microscaffolds and human adipose tissue-derived mesenchymal stem cells (hAT-MSCs). In addition, the purpose of this study is an approach of systematic bio-fusion method which means that human adipose tissue-derived mesenchymal stem cells (hAT-MSCs) could be cell-attached and osteogenic differentiated around Mg^{2+} ion-substituted biphasic calcium phosphate (Mg-BCP) micro-scaffold *in vitro*. Possibilities of hAT-MSC microcarrier and bone graft application for spherical Mg-BCP microscaffolds have also been investigated by an *in vivo* model.

2. Materials and Methods

2.1. Fabrication of Spherical Mg-BCP Microscaffolds. In order to prepare Mg-BCP microscaffolds, all processes were modified from our previous works [17]. Firstly, an appropriate amount (Mg/Ca molar ratio 0.01) of calcium nitrate tetrahydrate ($Ca(NO_3)_2{\cdot}4H_2O$) and magnesium nitrate hexahydrate ($Mg(NO_3)_2{\cdot}6H_2O$) was dissolved in distilled water by vigorously stirring at a rate of 1000 rpm. Diammonium hydrogen phosphate ($(NH_4)_2{\cdot}HPO_4$) solution was slowly added to the mixed solution of the calcium nitrate tetrahydrate and magnesium nitrate hexahydrate in order to obtain a nominal composition in terms of (Ca + Mg)/P ratio 1.602. The pH of the mixed solution was maintained at 11 by the addition of ammonium hydroxide (NH_4OH) solution. The coprecipitated suspension was discharged from the reactor and allowed to settle for 24 h for the maturation of precipitate. After 24 h, the precipitates were separated through vacuum filtration technique and dried at 80°C for 24 h in a drying oven.

To obtain the slurries of Mg-BCP, binder, dispersants and defoamer were used as organic additives and Mg-BCP precursor powders were slowly added into the organic additive solution via continuous attrition milling (400 RPM, 4 h). The as-prepared slurries were spray-dried with a rotary atomizer system. The spray-dried samples were placed in an alumina crucible and calcined at 1000°C for 24 h in air. The as-calcined Mg-BCP microscaffolds were sieved for the selection of appropriate sizes ranging from 45~75 μm (mesh nos. 200 and 325).

2.2. Characterization of Spherical Mg-BCP Microscaffolds. An X-ray diffractometer (XRD) at 40 kV and 40 mA with a scanning speed of 0.1°/min was adopted to identify the phases of Mg-BCP microscaffolds and compare them with pure BCPs. Microstructures and chemical compositions of samples were characterized using field emission scanning electron microscope (FE-SEM) and energy dispersive X-ray analyzer (SEM-EDX).

Hanks' balanced salt solution (HBSS), an extracellular solution with an ionic composition similar to human blood plasma, was used as the supporting solution for the Mg-BCP microscaffolds *in vitro* test. The simulated solution consisted of 8.00 g NaCl, 0.35 g $NaHCO_3$, 0.40 g KCl, 0.06 g KH_2PO_4, 0.10 g $MgCl_2{\cdot}6H_2O$, 0.14 g $CaCl_2$, 0.06 g $Na_2HPO_4{\cdot}2H_2O$, 0.06 g $MgSO_4{\cdot}7H_2O$, and 1.00 g glucose in 1000 mL distilled H_2O and had an initial pH of 7.4. Mg-BCP scaffolds were immersed in 50 mL of HBSS without organic species (pH 7.4), at 37°C in Teflon sealed polystyrene bottle for 1, 2, and 4 weeks. After immersing the samples in Hank's solution for 1, 2, and 4 weeks, Mg^{2+}, Ca^{2+}, and PO_4^{3-} concentrations of HBSS were measured using inductively coupled plasma atomic emission spectrometer (ICP-AES). After immersion for 1, 2, and 4 weeks, the scaffolds were rinsed 3 times with double-distilled water to remove residual HBSS and then immediately dried in vacuum desiccators at 21°C. The surface morphologies of the scaffolds before and after immersion in HBSS were analyzed using FE-SEM.

2.3. In Vitro and In Vivo Test of hAT-MSCs with Mg-BCP Microscaffolds. All protocols involving human subjects were approved by the Institutional Review Board of Pusan National University. The human adipose tissue-derived mesenchymal stem cells (hAT-MSCs) were isolated according to the methods described in previous studies [19]. Isolated cells were cultured in α-modified Eagle's medium (α-MEM), containing 10% fetal bovine serum (FBS).

The cells were detached using Hank's balanced salt solution containing 0.05% trypsin and 0.02% ethylenediaminetetraacetic acid (EDTA) to determine the rate of proliferation. The cells were plated on a 6-well plate at a density of 5×10^3 cells/well. MTT assay for 2 mg Mg-BCP microscaffolds was carried out to measure and evaluate cell survival and proliferation of mesenchymal stem cells (MSCs). MTT (3-(4,5-dimethylthiazol-2-yl)-2,5-diphenyltetrazolium bromide) was reduced to purple formazan in living cells. The absorbance of this colored solution could be measured at 560 nm in an ELISA reader. In statistical analysis, all results were presented as the mean standard error of the mean. Comparisons of cell viability between 2 groups of collagen and Mg-BCP were analyzed via Student's t-tests. Multiple group comparisons

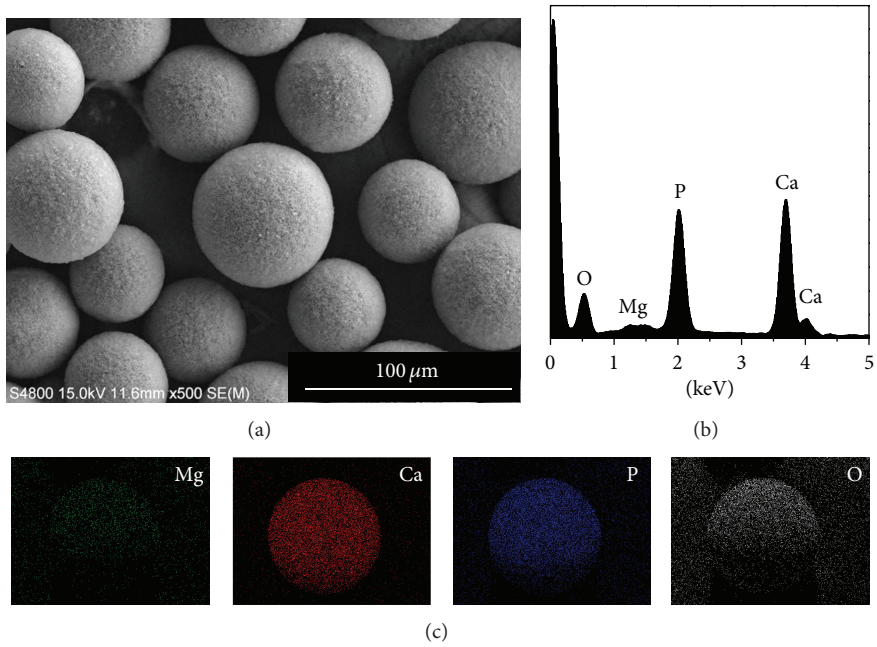

Figure 1: (a) FE-SEM micrographs, (b) SEM-EDX spectrum, and EDX mapping results of spherical Mg-BCP microscaffolds.

were conducted by lone-way analysis of variance with Tukey adjustments. P values <0.05 were considered statistically.

Osteogenic differentiation was induced through culturing of the cells for 14 days in osteogenic medium (10% FBS, 0.1 mM dexamethasone, 10 mM b-glycerophosphate, and 50 mM ascorbic acid in a-MEM), and extracellular matrix calcification was estimated using Alizarin Red S stain. Osteogenic differentiation was confirmed through the observation of the Alizarin Red stained area and density in 6-well dishes.

hAT-MSC-attached Mg-BCP scaffolds were evaluated qualitatively *in vivo* using critical-sized calvarial bone defects in adult (6 weeks old) severe combined immunodeficient (SCID) mice. The surgical procedures were performed in aseptic conditions under general anesthesia. Briefly, a linear incision (1 cm long) was made on the left side of the skull and the scalp was dissected to expose the calvaria. The periosteum was carefully peeled off and 2 lateral 4 mm wide calvarial bone defects were performed in each animal using a slow-speed dental drill with a 3 mm diameter trephine bur. To avoid tissue damage due to overheating, 0.9% saline was dripped onto the contact point between the bur and bone and great care was taken to avoid dura mater injury. hAT-MSC-attached Mg-BCP scaffolds were then implanted into one of the defect sites while the contralateral site was implanted with pure hAT-MSCs as a control. The animals were euthanized after 1 and 2 months by exposure to hyperbaric carbon dioxide. At each time point after 1 and 2 months, the skulls were harvested and fixed in 4% paraformaldehyde for 12 h. Calvaria were X-rayed using a volumetric computed tomography (CT) scanner at 50 kVp, 65 μA, and 470 ms per frame and then decalcified overnight with decalcifying solution (10% EDTA). Samples were then trimmed, processed, and embedded in paraffin wax. A micro-CT image of the mouse calvaria was taken using the CT scanner without changing the position of the animal's head. Paraffin-embedded samples were sectioned into 10 mm thick slices with a microtome. The surface morphologies of the as-implanted sample were analyzed using FE-SEM and SEM-EDX after *in vivo* test.

3. Results and Discussion

3.1. Mg-BCP Microscaffolds. Figure 1 shows FE-SEM image and SEM-EDX results of the spherical Mg-BCP microscaffolds. As shown in Figure 1(a), Mg-BCP microscaffolds had spherical morphologies after *in situ* coprecipitation, spray drying atomization, and calcination process. Result of SEM-EDX spectrum showed that Mg-BCP microscaffolds were mainly composed of Ca, P, O, and Mg atoms (Figure 1(b)). In addition, EDX mapping indicated that Mg atoms were uniformly spread out with the calcium phosphate elements (Figure 1(c)).

XRD patterns for as-synthesized spherical BCP and Mg-BCP microscaffolds are presented in Figure 2. As can be seen in Figure 2, all the obtained microscaffolds had both the β-TCP (JCPDS PDF no. 09-169) and HAp (JCPDS PDF no. 09-432) phase confirming the formation of biphasic mixtures. However, there is a difference in diffraction intensities of the peaks assigned to the β-TCP phase in Mg-BCPs compared to pure BCPs. These results could suggest that Mg^{2+} ions were preferentially incorporated into the β-TCP phase, replacing of Ca^{2+} ion (ionic radius ~0.99 Å) by Mg^{2+} ion (ionic radius ~0.65 Å), inducing a lattice contraction and respective displacement of the β-TCP reflections toward higher 2θ angles, as mentioned in the literature [26].

3.2. In Vitro Biodegradation and Bioactivity of Mg-BCP Microscaffolds in HBSS. Figure 3 shows the typical surface features of Mg-BCP microscaffolds after immersing in HBSS for 0,

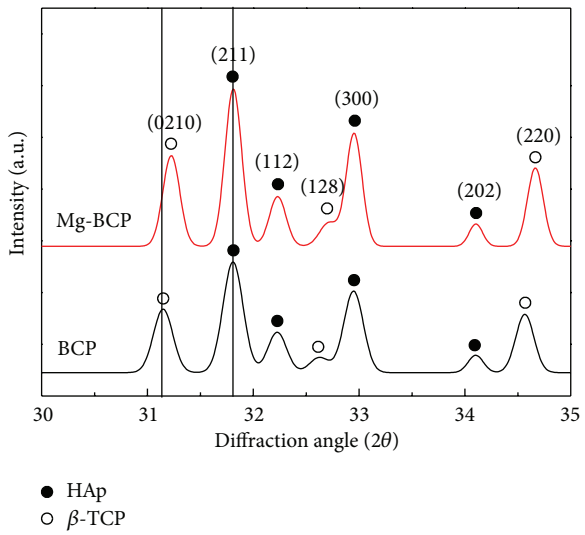

Figure 2: XRD patterns (•: HAp, JCPDS PDF no. 09-432, ○: β-TCP, JCPDS PDF no. 09-169) of spherical Mg-BCP microscaffolds.

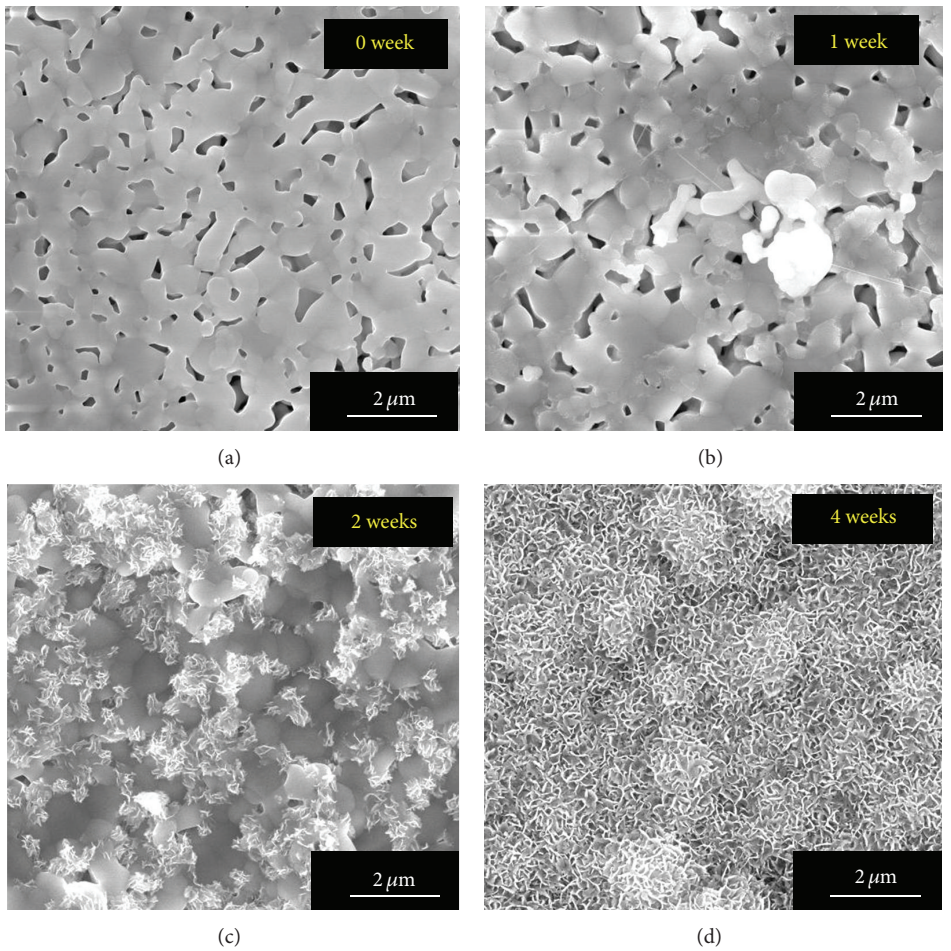

Figure 3: Surface morphologies of Mg-BCP microscaffolds after immersed in HBSS: (a) 0, (b) 1, (c) 2, and (d) 4 weeks.

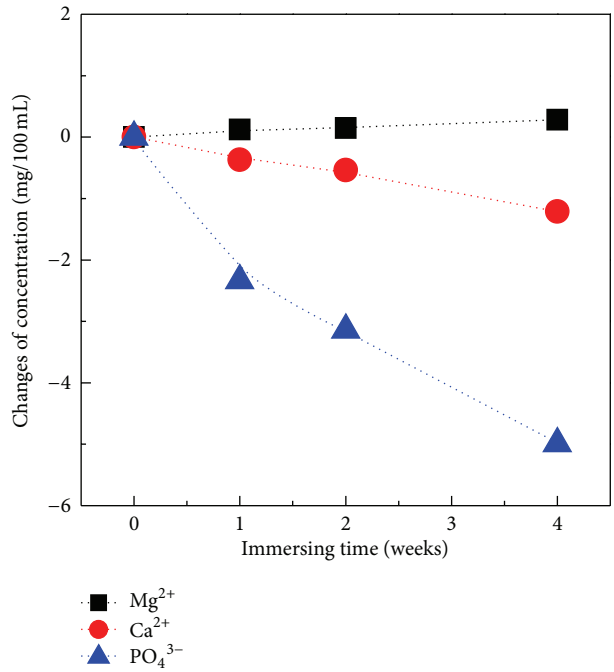

Figure 4: Change of Mg^{2+}, Ca^{2+}, and PO_4^{3-} ion concentrations in HBSS immersed with Mg-BCP microscaffolds during 4 weeks.

1, 2, and 4 weeks, respectively. As can be seen in Figure 3(a), the surface morphology of Mg-BCP microscaffolds showed primary particle-interconnected structure with micropores. The Mg-BCP microscaffolds were partially degraded during immersion in HBSS after 1 and 2 weeks (Figures 3(b) and 3(c)). The Mg-BCP microscaffolds, shown in Figure 3(d) were formed with individual flake-like nanocrystalline calcium deficient apatite (CDA) after 4 weeks.

The ICP-AES analysis reveals the changes of Mg^{2+}, Ca^{2+}, and PO_4^{3-} concentrations in HBSS after immersing the Mg-BCP microscaffolds, as shown in Figure 4. The Mg^{2+} ions were slowly released with increasing immersion time, which indicated that the Mg^{2+} ions were released from the β-TCP phase in Mg-BCP. On the other hand, the concentration of Ca^{2+} and PO_4^{3-} ions in HBSS continually decreased with increasing immersion time, suggesting that the decrease in concentration of Ca^{2+} and PO_4^{3-} ions might be a result of the formation of new CDA.

3.3. In Vitro Proliferation and Osteogenic Differentiation of hAT-MSCs with Mg-BCP Microscaffolds. Figure 5 shows *in vitro* biological properties of Mg-BCP microscaffolds related to hAT-MSCs. As can be seen in Figure 5(a), hAT-MSCs spread out around the surface of Mg-BCP microscaffolds, demonstrating the biocompatibility of Mg-BCP microscaffolds and had elongated phenotype for 3 days. Thus, cell attachment behaviors on the surface of Mg-BCP microscaffolds showed good biocompatibility indicated of hAT-MSCs growth and proliferation for 7 and 14 days, respectively. From the SEM image as shown in Figure 5(b), it was also observed that hAT-MSCs had clearly attached on the surface of Mg-BCP microscaffolds. Such behaviors might be caused to existence of blast related to hAT-MSCs in pores of Mg-BCP microscaffolds (Figure 5(c)). Cell viability results in Figure 5(d) indicated that Mg-BCP microscaffolds had no cytotoxic effects on hAT-MSCs and have good biocompatibility, which are consistent with the results presented in Figures 5(a), 5(b), and 5(c). In the osteoconductivity evaluation, hAT-MSCs with Mg-BCP microscaffolds showed enhanced osteogenic cell differentiation (Alizarin Red staining area was the osteogenic cell differentiation of hAT-MSCs) compared to pure hAT-MSCs as shown in Figure 6(a). From optical microscopy imaging as shown in Figure 6(b), it was also observed that osteogenic differentiated-hAT-MSCs have clearly attached on the surface of Mg-BCP microscaffolds.

3.4. In Vivo Test in Bone Defects of SCID Mice. In biological osteoconductivity evaluation of Mg-BCP microscaffolds via *in vivo* test, new bone generation behavior within the oval bone defects of SCID mice showed extreme difference in results between the two types of implant material. As shown in Figure 7, after 2 months *in vivo*, micro-CT images of sites implanted with hAT-MSCs containing Mg-BCP microscaffolds showed relative high-dense area due to new bone mineralization whereas the area implanted with pure hAT-MSCs had no new bone mineralization. Figure 8 shows FE-SEM image and SEM-EDX results of hAT-MSCs/Mg-BCP-implanted sample after 2 months. As shown in Figure 8(a), Mg-BCP micro-scaffold maintained its spherical morphology after the *in vivo* test and small particles were noted on the surface of the as-implanted sample due to the formation of new bone around the scaffold. In addition, result of

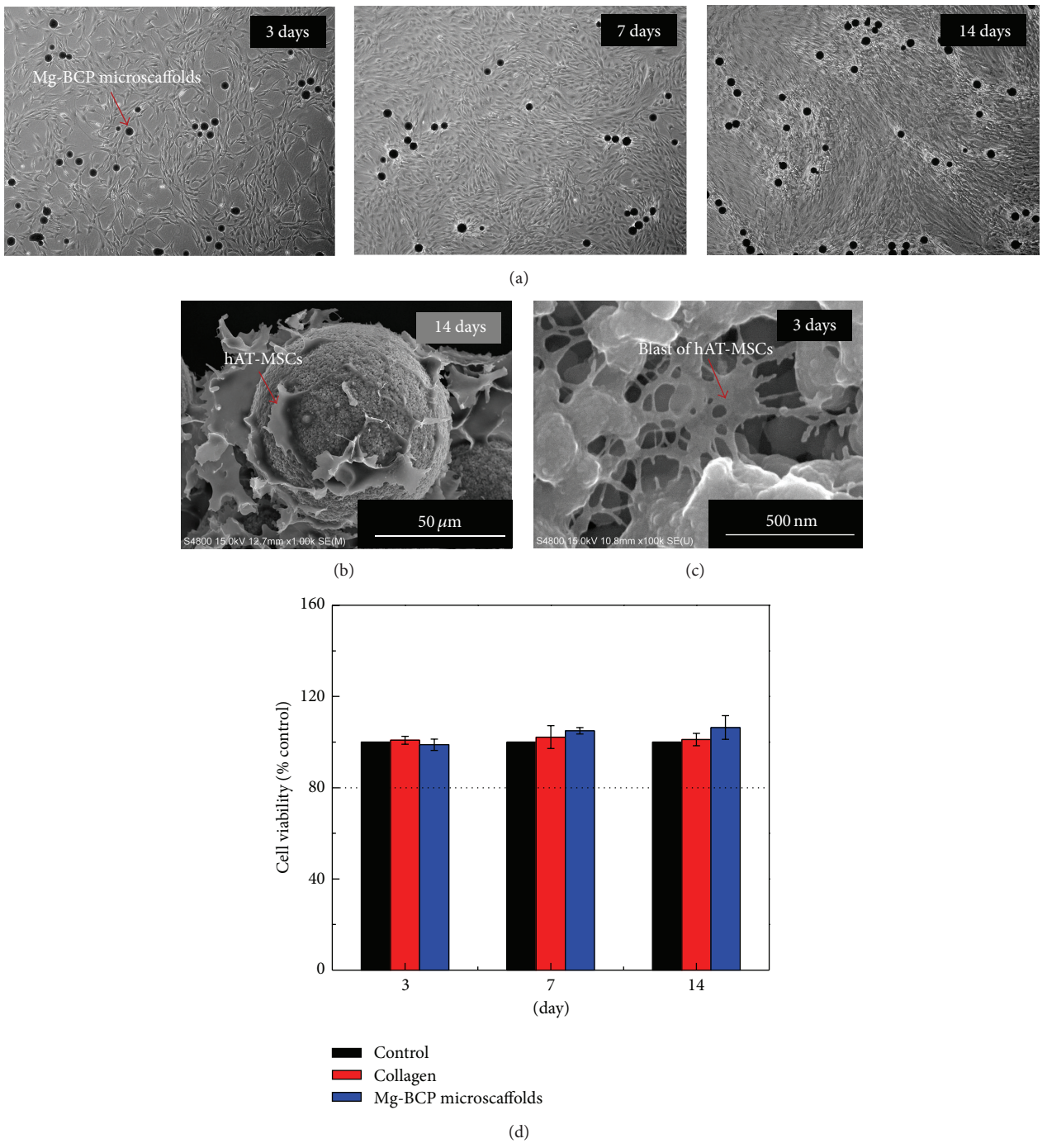

FIGURE 5: *In vitro* biological properties of hAT-MSCs with Mg-BCP microscaffolds: (a) morphological features of hAT-MSCs growth and proliferation, (b) SEM micrographs of hAT-MSCs-attached Mg-BCP microscaffolds, (c) blast of hAT-MSCs in micropore structure of Mg-BCP microscaffolds, and (d) cell viability results.

SEM-EDX mapping also shows that chemical composition atoms, indicated around the sample of implanted Mg-BCP microscaffolds, might be related to the formation of new generation bone and similar to main composition (Ca, P, and O atoms) of Mg-BCP micro-scaffold (Figure 8(b)). It can be affirmed from these *in vivo* results that Mg-BCP microscaffolds were not only bioactive 3D extracellular tissue materials with enhanced osteoconductivity but are also suitable cell microcarriers for cell attachment and proliferation of hAT-MSCs.

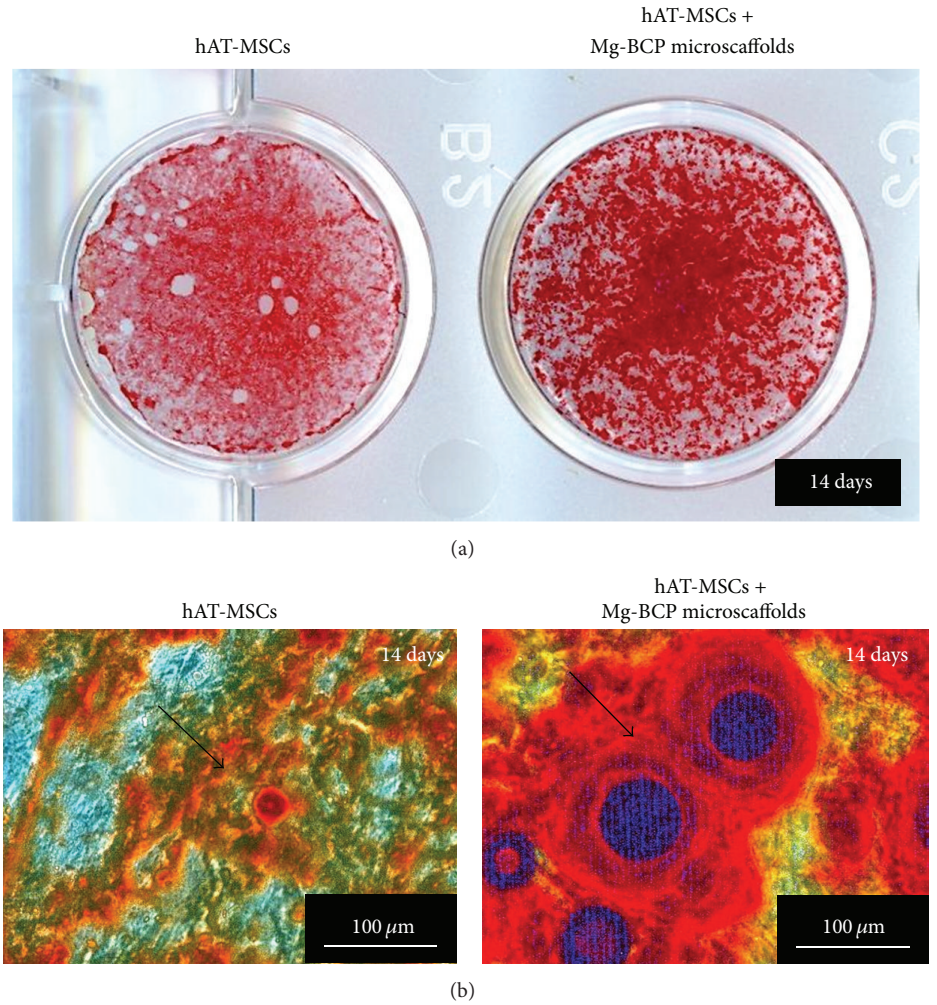

Figure 6: Osteogenic cell differentiation of hAT-MSCs after 14 days: (a) Alizarin Red staining area in dishes and (b) optical microscopy images.

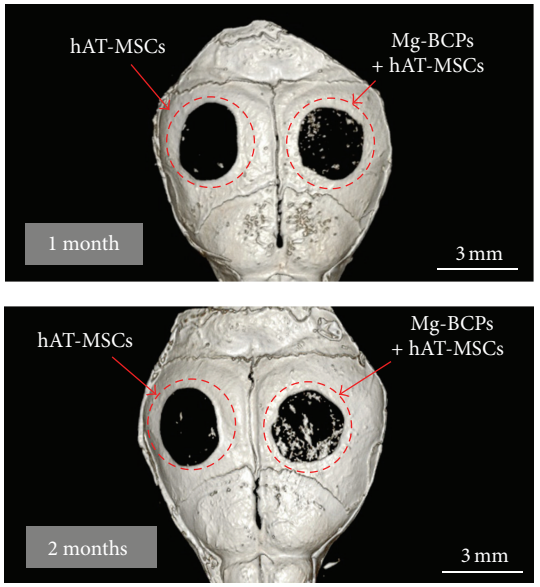

Figure 7: Micro-CT images of the mouse skulls after 2 months *in vivo*.

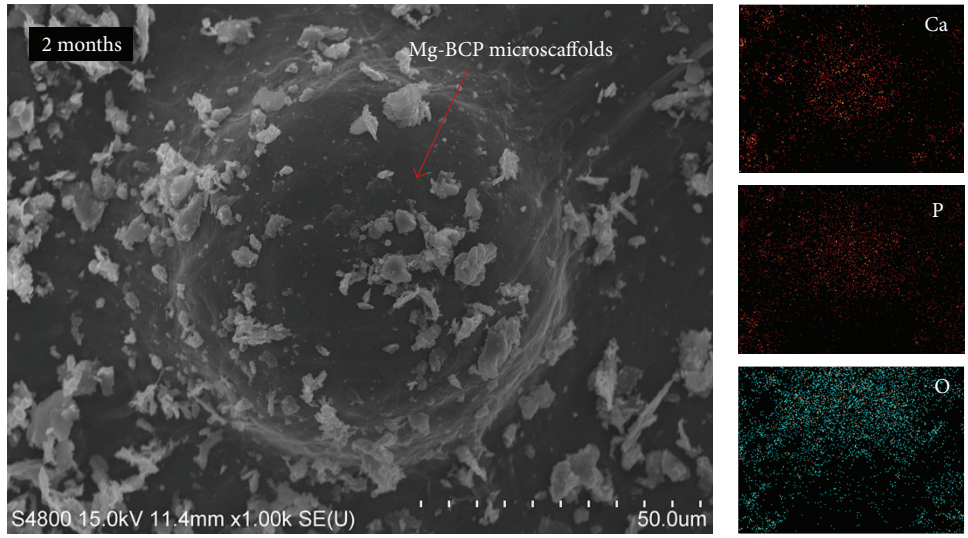

(a) (b)

Figure 8: (a) FE-SEM micrographs and (b) SEM-EDX mapping results from as-implanted sample after 2 months *in vivo*.

4. Conclusions

Spherical Mg-BCP microscaffolds were successfully prepared using *in situ* coprecipitation and rotary spray drying atomization process. After immersion for 4 weeks in HBSS, Mg-BCP microscaffolds showed enhanced biodegradation and bioactivity. These biodegradation and bioactivity of Mg-BCP microscaffolds during soaking in HBSS results in the reduction of stability of the β-TCP structure due to distortion of crystal structure by the substitution of Mg^{2+} ion into Ca^{2+} sites in BCP, which has a different crystal structure. In this study, it was observed that osteogenic-differentiated hAT-MSCs have clearly attached on the surface of Mg-BCP microscaffolds. Therefore, Mg-BCP microscaffolds having enhanced biological properties related to biocompatibility and osteoconductivity could have potential application as hAT-MSCs microcarriers as seen from the *in vitro* and *in vivo* results. However, additional experimental research is needed to verify more detailed mechanism and to determine the mutual behaviors between Mg-BCP microscaffolds and hAT-MSCs.

Acknowledgments

This work was supported by the Industrial Infrastructure Program through the Korea Institute for Advancement of Technology (KIAT) grant funded by the Korea Government Ministry of Trade, Industry and Energy (no. N009700001). This research was also a part of the project titled "Development of Key Technology in Seawater Desalination Using Gas Hydrate Process" funded by the Ministry of Oceans and Fisheries and Korea Institute of Industrial Technology.

References

[1] G. Daculsi, "Biphasic calcium phosphate concept applied to artificial bone, implant coating and injectable bone substitute," *Biomaterials*, vol. 19, no. 16, pp. 1473–1478, 1998.

[2] B. H. Fellah, O. Gauthier, P. Weiss, D. Chappard, and P. Layrolle, "Osteogenicity of biphasic calcium phosphate ceramics and bone autograft in a goat model," *Biomaterials*, vol. 29, no. 9, pp. 1177–1188, 2008.

[3] H. Yuan, C. A. van Blitterswijk, K. de Groot, and J. D. de Bruijn, "Cross-species comparison of ectopic bone formation in biphasic calcium phosphate (BCP) and hydroxyapatite (HA) scaffolds," *Tissue Engineering*, vol. 12, no. 6, pp. 1607–1615, 2006.

[4] M. P. Ginebra, M. Espanol, E. B. Montufar, R. A. Perez, and G. Mestres, "New processing approaches in calcium phosphate cements and their applications in regenerative medicine," *Acta Biomaterialia*, vol. 6, no. 8, pp. 2863–2873, 2010.

[5] F. Tamimi, J. Torres, C. Kathan et al., "Bone regeneration in rabbit calvaria with novel monetite granules," *Journal of Biomedical Materials Research Part A*, vol. 87, no. 4, pp. 980–985, 2008.

[6] W. Paul, J. Nesamony, and C. P. Sharma, "Delivery of insulin from hydroxyapatite ceramic microspheres: preliminary in vivo studies," *Journal of Biomedical Materials Research*, vol. 61, no. 4, pp. 660–662, 2002.

[7] S. Labbaf, O. Tsigkou, K. H. Müller, M. M. Stevens, A. E. Porter, and J. R. Jones, "Spherical bioactive glass particles and their interaction with human mesenchymal stem cells in vitro," *Biomaterials*, vol. 32, no. 4, pp. 1010–1018, 2011.

[8] Y. Gonda, K. Ioku, Y. Shibata et al., "Stimulatory effect of hydrothermally synthesized biodegradable hydroxyapatite granules on osteogenesis and direct association with osteoclasts," *Biomaterials*, vol. 30, no. 26, pp. 4390–4400, 2009.

[9] D. J. Misiek, J. N. Kent, and R. F. Carr, "Soft tissue responses to hydroxylapatite particles of different shapes," *Journal of Oral and Maxillofacial Surgery*, vol. 42, no. 3, pp. 150–160, 1984.

[10] B. Chang, C. Lee, K. Hong et al., "Osteoconduction at porous hydroxyapatite with various pore configurations," *Biomaterials*, vol. 21, no. 12, pp. 1291–1298, 2000.

[11] S. V. Dorozhkin, "Biphasic, triphasic and multiphasic calcium orthophosphates," *Acta Biomaterialia*, vol. 8, no. 3, pp. 963–977, 2012.

[12] E. Boanini, M. Gazzano, and A. Bigi, "Ionic substitutions in calcium phosphates synthesized at low temperature," *Acta Biomaterialia*, vol. 6, no. 6, pp. 1882–1894, 2010.

[13] S. Kannan, S. I. Vieira, S. M. Olhero et al., "Synthesis, mechanical and biological characterization of ionic doped carbonated hydroxyapatite/β-tricalcium phosphate mixtures," *Acta Biomaterialia*, vol. 7, no. 4, pp. 1835–1843, 2011.

[14] L. Saldaña, S. Sánchez-Salcedo, I. Izquierdo-Barba et al., "Calcium phosphate-based particles influence osteogenic maturation of human mesenchymal stem cells," *Acta Biomaterialia*, vol. 5, no. 4, pp. 1294–1305, 2009.

[15] A. Bigi, G. Falini, E. Foresti, M. Gazzano, A. Ripamonti, and N. Roveri, "Rietveld structure refinements of calcium hydroxylapatite containing magnesium," *Acta Crystallographica Section B*, vol. 52, no. 1, pp. 87–92, 1996.

[16] A. Yasukawa, S. Ouchi, K. Kandori, and T. Ishikawa, "Preparation and characterization of magnesium-calcium hydroxyapatites," *Journal of Materials Chemistry*, vol. 6, no. 8, pp. 1401–1405, 1996.

[17] T. W. Kim, H. S. Lee, D. H. Kim et al., "In situ synthesis of magnesium-substituted biphasic calcium phosphate and in vitro biodegradation," *Materials Research Bulletin*, vol. 47, no. 9, pp. 2506–2512, 2012.

[18] J. H. Lee, J. W. Rhie, D. Y. Oh, and S. T. Ahn, "Osteogenic differentiation of human adipose tissue-derived stromal cells (hASCs) in a porous three-dimensional scaffold," *Biochemical and Biophysical Research Communications*, vol. 370, no. 3, pp. 456–460, 2008.

[19] Y. J. Kim, S. W. Bae, S. S. Yu, Y. C. Bae, and J. S. Jung, "miR-196a regulates proliferation and osteogenic differentiation in mesenchymal stem cells derived from human adipose tissue," *Journal of Bone and Mineral Research*, vol. 24, no. 5, pp. 816–825, 2009.

[20] J. I. Huang, S. R. Beanes, M. Zhu, H. P. Lorenz, M. H. Hedrick, and P. Benhaim, "Rat extramedullary adipose tissue as a source of osteochondrogenic progenitor cells," *Plastic and Reconstructive Surgery*, vol. 109, no. 3, pp. 1033–1041, 2002.

[21] P. A. Zuk, M. Zhu, H. Mizuno et al., "Multilineage cells from human adipose tissue: implications for cell-based therapies," *Tissue Engineering*, vol. 7, no. 2, pp. 211–228, 2001.

[22] P. A. Zuk, M. Zhu, P. Ashjian et al., "Human adipose tissue is a source of multipotent stem cells," *Molecular Biology of the Cell*, vol. 13, no. 12, pp. 4279–4295, 2002.

[23] J. Shi, X. Zhang, Y. Pi, J. Zhu, C. Zhou, and Y. Ao, "Nanopolymers delivery of the bone morphogenetic protein-4 plasmid to mesenchymal stem cells promotes articular cartilage repair in vitro and in vivo," *Journal of Nanomaterials*, vol. 2012, Article ID 236953, 9 pages, 2012.

[24] K. S. Moon, S. H. Yu, J. M. Bae, and S. Oh, "Biphasic osteogenic characteristics of human mesenchymal stem cells cultured on TiO_2 nanotubes of different diameters," *Journal of Nanomaterials*, vol. 2012, Article ID 252481, 8 pages, 2012.

[25] G. Chen, W. Song, and N. Kawazoe, "Dependence of spreading and differentiation of mesenchymal stem cells on micropatterned surface area," *Journal of Nanomaterials*, vol. 2011, Article ID 265251, 9 pages, 2011.

[26] S. Kannan, I. A. F. Lemos, J. H. G. Rocha, and J. M. F. Ferreira, "Synthesis and characterization of magnesium substituted biphasic mixtures of controlled hydroxyapatite/β-tricalcium phosphate ratios," *Journal of Solid State Chemistry*, vol. 178, no. 10, pp. 3190–3196, 2005.